

# Fully Spiking Denoising Diffusion Implicit Models

Ryo Watanabe<sup>1</sup>, Yusuke Mukuta<sup>1,2</sup>, Tatsuya Harada<sup>1,2</sup>

<sup>1</sup> The University of Tokyo

<sup>2</sup> RIKEN

{r-watanabe, mukuta, harada}@mi.t.u-tokyo.ac.jp

## Abstract

*Spiking neural networks (SNNs) have garnered considerable attention owing to their ability to run on neuromorphic devices with super-high speeds and remarkable energy efficiencies. SNNs can be used in conventional neural network-based time- and energy-consuming applications. However, research on generative models within SNNs remains limited, despite their advantages. In particular, diffusion models are a powerful class of generative models, whose image generation quality surpass that of the other generative models, such as GANs. However, diffusion models are characterized by high computational costs and long inference times owing to their iterative denoising feature. Therefore, we propose a novel approach fully spiking denoising diffusion implicit model (FSDDIM) to construct a diffusion model within SNNs and leverage the high speed and low energy consumption features of SNNs via synaptic current learning (SCL). SCL fills the gap in that diffusion models use a neural network to estimate real-valued parameters of a predefined probabilistic distribution, whereas SNNs output binary spike trains. The SCL enables us to complete the entire generative process of diffusion models exclusively using SNNs. We demonstrate that the proposed method outperforms the state-of-the-art fully spiking generative model.*

## 1. Introduction

Spiking neural networks (SNNs) are neural networks designed to mimic the signal transmission in the brain [53]. Information in SNNs is represented as binary spike trains that are subsequently transmitted by neurons. SNNs have not only biological plausibility but also enormous computational efficiency. Owing to their potential to operate with extremely low energy consumption and high-speed performance [6, 44] on neuromorphic devices [6, 11, 41], SNNs have garnered significant attention in recent years. However, the research on image generation models within SNNs remains limited [25].

Diffusion models [22, 49] are types of generative mod-

els trained to obtain the reverse process of a predefined forward process that iteratively adds noise to the given data. The generative process is achieved by iteratively denoising a given noise sample from a completely random prior distribution. Diffusion models have been actively explored, as it has been reported that they can generate high-quality images, outperforming state-of-the-art image generation models [13, 22] such as GANs [3, 15, 26]. However, diffusion models incur high computational costs and long inference times because of the iterative denoising of generative processes. Therefore, SNNs are promising candidates for accelerating the inference of diffusion models by utilizing SNNs capability for high-speed and low-energy-consumption computation. However, although many studies on diffusion models have been published in the field of conventional artificial neural networks (ANNs) [1, 9, 13, 19, 22, 42, 46, 49], research on diffusion models in SNNs is limited. To the best of our knowledge, only two studies exist for diffusion models that use SNNs [4, 35].

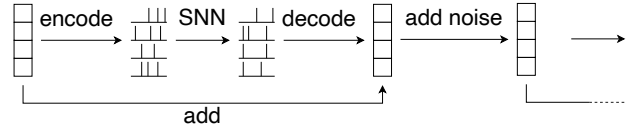
The challenge in developing diffusion models for SNNs lies in designing the generation process. For example, DDPM [22], which is the basis of many recent studies on image-generation diffusion models [9, 13, 39, 42, 46], uses Gaussian noise in the forward process. Therefore, the generative process is defined as Gaussian. A neural network is used to estimate the parameters of the Gaussian and a next step denoised image is sampled from it. However, in the framework of SNNs, the outputs of the spiking neurons are binary spike trains; therefore, we cannot directly estimate the Gaussian parameters, which are real values, using SNNs. Other diffusion models using different probabilistic distributions, such as the categorical distribution [1, 19] or gamma distribution [38] also have the same problem because they use a neural network to estimate the real-valued parameters of the probabilistic distribution. To use an SNN for diffusion models naively, we must decode the output of the SNN to calculate the parameters of the probabilistic distribution and encode the sampled image from the distribution to feed it to the SNN in the next denoising step. Although these steps are repeated many times, *e.g.*

1000 times, to obtain the final denoised result, the subsequent sampling process after decoding cannot be performed within the framework of SNNs. In addition, this decoding process hinders the full utilization of SNNs because we must wait until the final spike is emitted, whereas the output of the SNN model is subsequently emitted as spike trains over time (Fig. 1a). Existing studies on SNN diffusion have not solved this problem. Both SDDPM [4] and Spiking-Diffusion [35] must decode the output of the SNN model from spike-formed data to the image output and sample from the calculated probabilistic distribution in each denoising step. Therefore, their work cannot be treated as a "fully spiking" generative model which means that it can be completed by SNN alone while they partially use SNNs.

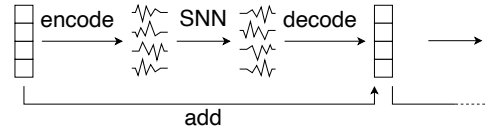
Here, we propose fully spiking denoising diffusion implicit model (FSDDIM) solving the problem (Fig. 1d and Fig. 1e). In this study, we adopted DDIM [49], which is a deterministic generative process of Gaussian-based diffusion models, to eliminate the need for random sampling in each denoising step. A single step of denoising in DDIM is represented by a linear combination of the input and output of the neural network. Hence, if we naively implement a DDIM with an SNN, we must decode the output of the SNN to calculate the linear combination, and encode the result again to feed it into the SNN in the next denoising step. This is the same problem as in existing studies.

To solve this problem, we propose a novel technique called synaptic current learning (SCL). In SCL, we consider synaptic currents as model outputs instead of spike trains [8, 27, 31, 60] (Fig. 1b). Synaptic currents are real-valued signals that are the sum of spikes multiplied by the synaptic weight between the presynaptic and postsynaptic neurons. At the same time, we use linear functions for the encoder and decoder, which map an image to the synaptic currents and vice versa. This linear encoding and decoding scheme enabled us to compute scalar multiplication in a linear combination of DDIM with synaptic currents, rather than a decoded image (Fig. 1b). Finally, we introduce SCL loss. SCL loss ensured that the output of the SNN model could be reconstructed after decoding and encoding. Owing to this loss, we could remove the encoding and decoding processes in each denoising step and complete the entire generative process using the SNN alone (Fig. 1d). Additionally, we showed that our model, which outputs synaptic currents, can be equivalently regarded as a model that outputs spike trains by fusing the linear combination weights and the first and last convolutional layers into a single convolutional layer (Fig. 1e).

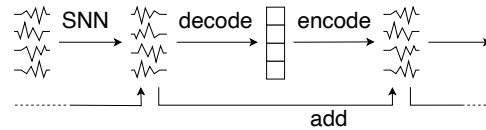
To the best of our knowledge, FSDDIM is the first to complete the entire generative process of diffusion models exclusively using SNNs. Finally, we demonstrate that the proposed method outperforms the state-of-the-art fully spiking image generation model for SNNs.



(a) Naively implemented DDPM with an SNN using spikes as input/output. Vertically aligned rectangles represent a vector in the image space. The decoding process requires wait for the final spike emitted.



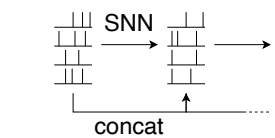
(b) Naively implemented DDIM with an SNN using synaptic currents as input/output. DDIM eliminate the need for random noise in each step. The input and output of the SNN are synaptic currents.



(c) DDIM in which the linear combination is computed in signal space via linear encoder and decoder



(d) FSDDIM with an SNN using synaptic currents as input/output



(e) FSDDIM with an SNN using spike trains as input/output

Figure 1. Comparison of the generative process of DDPM, DDIM and FSDDIM.

We summarize our contributions as follows:

- We propose a novel approach named Fully Spiking Denoising Diffusion Implicit Models (FSDDIM) to build a diffusion model within SNNs.
- We introduce the Synaptic Current Learning (SCL) adopting synaptic currents as model outputs and linear encoding and decoding scheme. We show that the SCL loss enables us to complete the entire generative process of our diffusion model exclusively using SNNs.
- We demonstrate that our proposed method outperforms the state-of-the-art fully spiking image generation model in terms of the quality of generated images and the number of time steps.

## 2. Related work

### 2.1. Spiking neural networks

SNNs model the features of a biological brain, in which the signal is emitted as spike trains, which are time-series binary data. The emitted spikes change the membrane potential of the postsynaptic neuron; when the membrane potential reaches a threshold value, the neuron emits a spike. The

membrane potential is reset to the resting potential after the spike emission. We use the iterative leaky integrate-and-fire (LIF) model [56] in this study. The iterative LIF model is the first-order Euler approximation of the LIF model [50] and is defined as follows:

$$u_s = \tau_{decay} u_{s-1} + I_s \quad (1)$$

where  $u_s$  is the membrane potential at the time step  $s = 1, \dots, S$ .  $S$  is the number of time steps.  $\tau_{decay}$  is the decay constant and  $I_s$  is the synaptic current at time step  $s$ . The neuron emits a spike when the membrane potential  $u_s$  reaches the threshold value  $V_{th}$  and the membrane potential is reset to 0 after emitting the spike. This is expressed as follows:

$$u_{s,n}^i = \tau_{decay} u_{s-1,n}^i (1 - o_{s-1,n}^i) + I_{s,n-1}^i \quad (2)$$

$$o_{s,n}^i = \begin{cases} 1 & \text{if } u_{s,n}^i \geq V_{th} \\ 0 & \text{otherwise} \end{cases} \quad (3)$$

Here,  $u_{s,n}^i$  and  $o_{s,n}^i$  are the membrane potential and the output of the  $i$ th neuron in the  $n$ th layer at time step  $s$  respectively.

The synaptic current  $I_{s,n-1}^i$  is the weighted sum of all spikes transmitted by the neurons of the previous layer and is calculated by

$$I_{s,n-1}^i = \sum_j w_j o_{s,n-1}^j \quad (4)$$

$j$  is the index of neurons connected to the neuron and  $w_j$  is the synaptic weight of each connection.  $o_{s,n-1}^j$  is the output of the  $j$ th neuron at time step  $s$  in the  $n-1$ th layer.

## 2.2. Training of SNNs

Learning algorithms for SNNs have been actively investigated in recent years. Legenstein *et al.* [33] used spike timing-dependent plasticity (STDP) [5] to train SNNs. Diehl *et al.* [14] proposed an unsupervised learning method using STDP and achieved 95% accuracy on MNIST [30]. Recently, backpropagation has been widely used to train SNNs [2, 10, 16, 18, 32, 55, 59] and these methods have achieved high performance compared with other existing methods. As the firing mechanisms in spiking neurons, such as those in Eq. (3), are non-differentiable, surrogate gradient functions are used to make backpropagation possible. Zenke *et al.* [58] systematically demonstrated the robustness of surrogate gradient learning.

In this study, we used surrogate gradient learning to train SNNs. We used a surrogate gradient function similar to that in [55, 58] which is defined as

$$\frac{\partial o_{s,n}^i}{\partial u_{s,n}^i} = \max \left( 1 - \frac{1}{a} |u_{s,n}^i - V_{th}|, 0 \right) \quad (5)$$

## 2.3. Diffusion models

Diffusion models are generative models that generate the original data via iterative denoising. Ho *et al.* [22] proposed the denoising diffusion probabilistic model (DDPM) and demonstrated the high-quality image generation ability of diffusion models. This work was followed by numerous other reported studies in later years [13, 19, 39, 42, 46, 49]. The forward process of DDPM is a Markov chain that gradually adds Gaussian noise.

$$q(x_t | x_{t-1}) = \mathcal{N}(x_t; \sqrt{\alpha_t} x_{t-1}, (1 - \alpha_t)I) \quad (6)$$

$x_0$  is the given data and iteratively adds noise defined in Eq. (6) from  $t = 1$  to  $T$  such that  $x_T$  follows a standard Gaussian distribution  $p(x_T) = \mathcal{N}(x_T; 0, I)$ . This definition enables us to sample  $x_t$  in closed form using  $\bar{\alpha}_t = \prod_{s=1}^t \alpha_s$

$$q(x_t | x_0) = \mathcal{N}(x_t; \sqrt{\bar{\alpha}_t} x_0, (1 - \bar{\alpha}_t)I) \quad (7)$$

While the training objective of reverse process  $p_\theta(x_0:T)$  is derived from the variational bound on negative log likelihood  $\mathbb{E}[-\log p_\theta(x_0)]$ , Ho *et al.* [22] and later works [9, 20] found that the loss function Eq. (8) improves the performance instead of the variational bound.

$$L_\gamma = \sum_{t=1}^T \gamma_t \mathbb{E} \left[ \left\| \epsilon - \epsilon_\theta^{(t)} \left( \sqrt{\bar{\alpha}_t} x_0 + \sqrt{1 - \bar{\alpha}_t} \epsilon \right) \right\|^2 \right] \quad (8)$$

where  $\epsilon$  is a noise sampled from the standard Gaussian distribution  $\mathcal{N}(0, I)$  and  $\epsilon_\theta^{(t)}$  is the noise estimated using a neural network.

Song *et al.* [49] studied a non-Markovian definition of diffusion models and showed that the variational inference objective under their definition is equivalent to the weighted loss function of DDPM in Eq. (8). Remarkably, their generative process allows deterministic sampling, called denoising diffusion implicit model (DDIM):

$$x_{t-1} = \sqrt{\bar{\alpha}_{t-1}} \left( \frac{x_t - \sqrt{1 - \bar{\alpha}_t} \epsilon_\theta^{(t)}(x_t)}{\sqrt{\bar{\alpha}_t}} \right) + \sqrt{1 - \bar{\alpha}_{t-1}} \epsilon_\theta^{(t)}(x_t) \quad (9)$$

They also showed that DDIM could generate better-quality images in fewer steps than DDPM.

Other studies used different forms of the target predicted by neural networks, such as directly estimating the original image  $x_0$  [19, 47] and velocity [47]. Because  $x_t$  can be sampled from Eq. (7), the relationship between  $x_t$ ,  $\epsilon$  and  $x_0$  can be written as

$$x_t = \sqrt{\bar{\alpha}_t} x_0 + \sqrt{1 - \bar{\alpha}_t} \epsilon \quad (10)$$

Velocity  $v_t$  is defined as follows:

$$v_t = \sqrt{\bar{\alpha}_t} \epsilon - \sqrt{1 - \bar{\alpha}_t} x_0 \quad (11)$$

Regardless of the targets  $\epsilon$ ,  $x_0$  and  $v_t$ , the denoising step of DDIM is represented as a linear combination of the input and output of the neural network  $f_{\text{NN}}(x_t, t)$ :

$$x_{t-1} = a_t x_t + b_t f_{\text{NN}}(x_t, t) \quad (12)$$

where  $a_t$  and  $b_t$  are constants calculated from  $\bar{\alpha}_t$  and  $\bar{\alpha}_{t-1}$ .

## 2.4. Spiking diffusion models

Cao *et al.* [4] developed the spiking denoising diffusion probabilistic model (SDDPM), which simply replaced the U-Net [43, 48] used in DDPM [22] with an SNN called Spiking U-Net to enjoy the low energy consumption of SNNs. They additionally proposed threshold guidance to efficiently train the Spiking U-Net by adjusting the threshold  $V_{th}$ . They reported that SDDPM outperformed other image generation models of SNNs [25, 35]. However, it is problematic to treat their work as a "fully spiking" generative model which means that it can be completed by SNN alone. When calculating a single step of denoising in SDDPM, we first need to encode the input image into spike-formed data that SNNs can accept. We then decode the output of the Spiking U-Net from the spike-formed data to the image output. Finally, we calculate the parameters of the Gaussian distribution and sample the next step input image in the same manner as DDPM. As this calculation is performed after decoding, the following sampling process cannot be performed within the SNN.

Spiking-Diffusion [35], another existing SNN diffusion model, uses discrete diffusion models [1] instead of Gaussian-based diffusion models. To obtain a discrete representation of the dataset that they wanted to reproduce, they proposed a vector-quantized spiking variational encoder. However, they also calculated the denoising step by decoding the output of the SNN and sampling it from the calculated probabilistic distribution. Therefore, their study could not be completed using SNNs alone.

## 3. Method

SNNs handle spike trains and binary time-sequential data because the outputs of a spiking neuron are binary spike trains. However, many widely studied image-generation-diffusion models based on a Gaussian noise distribution [13, 22, 37, 39, 42, 46] require a neural network to estimate a real-valued target. Therefore, it is difficult to apply these diffusion models to SNNs.

Our model adopts Gaussian-based diffusion models to make it possible to incorporate knowledge from numerous studies on Gaussian-based diffusion models [7, 9, 13, 20, 24, 39, 47]. At the same time, our model can perform the entire generative process exclusively using SNNs, which is a crucial capability to ensure seamless integration with neuromorphic devices to enjoy the benefits of low energy consumption and high-speed calculation in the future.

## 3.1. Model overview

We describe our pipeline in Fig. 2. We use DDIM [49] as the basis of our diffusion model. DDIM is a deterministic generative process of Gaussian-based diffusion models. In inference phase, while a single denoising step of DDIM is computed by a linear combination of the input and output of a neural network, we enable our SNN model to calculate it without decoding the output of the SNN to original image space by proposed SCL.

At first, we incorporate an idea to regard synaptic currents as model outputs instead of spike trains. The synaptic currents are real-valued signals calculated by Eq. (4). The idea of using synaptic currents as the model output is not new and has been used in previous studies. Some studies that solved classification problems with SNNs [27, 31] used synaptic currents to calculate the final prediction by accumulating them using the membrane potential of non-firing neurons. Zheng *et al.* [60] also accumulated synaptic currents but averaged them over time. Cherdo *et al.* [8] proposed SRSNN which uses SNN as a recurrent neural network and directly minimizes the synaptic currents and target values.

Next, in the following section, we analyze DDIM naively implemented with an SNN in which the input is encoded to synaptic currents and the output is decoded to the original image space (Fig. 1b). As a result, we show that the encoding and decoding process can be removed by introducing the SCL loss utilizing linear encoder and decoder. In this way, the denoising step can be completed by a linear combination of the input and output synaptic currents of the SNN (Fig. 1d). This linear combination is processed independently for each time step, like ResNet in SNNs [17, 23, 51, 60]. Therefore, our diffusion model can process the denoising step without a delay in decoding the output of the SNN or by depending on modules other than SNNs. Additionally, we show that our model which outputs synaptic currents can be equivalently regarded as a model which outputs spike trains by fusing the linear combination weights and the first and last convolutional layer into a single convolutional layer (Fig. 1e). We call our diffusion model FSDDIM.

## 3.2. SCL for SNN diffusion

In this section, we describe how to train an SNN for FSDDIM and introduce SCL. First, we begin with the regular DDIM [49]. A single step in the generative process of DDIM is represented as Eq. (12).

Next, we consider replacing the neural network  $f_{\text{NN}}$  with an SNN  $f_{\text{SNN}}$  but use encoder  $f_{\text{enc}}$  and decoder  $f_{\text{dec}}$  to convert values in the original image space into time sequence signals that the SNNs take as inputs and outputs, and vice versa. Because our SNN model outputs synaptic currents, we define the encoder  $f_{\text{enc}}(\cdot)$  as a function that

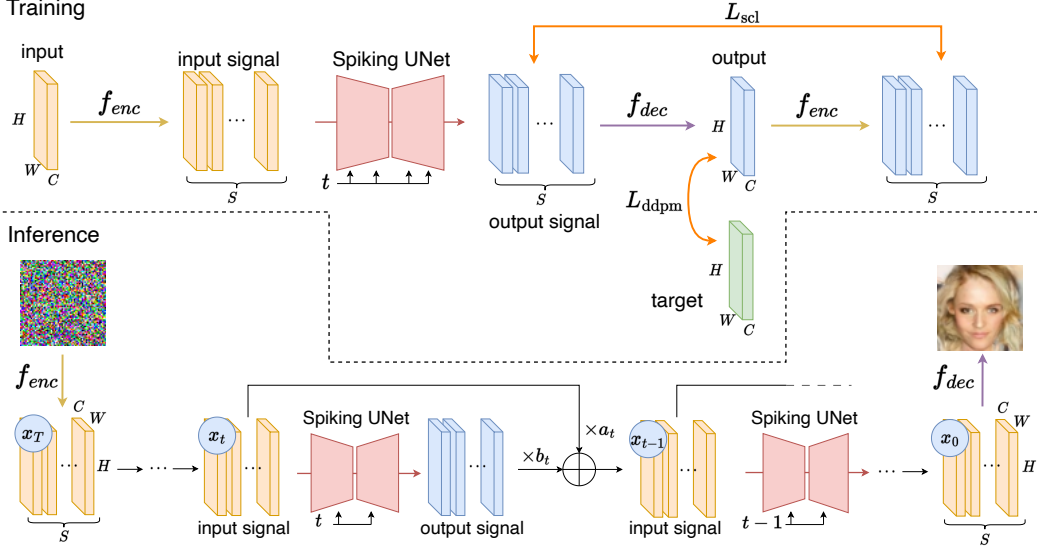


Figure 2. The overview of our proposed method.

maps an image  $x \in \mathbb{R}^{H \times W \times C}$ , with the shape of  $H \times W$  and  $C$  channels, to the sequential synaptic current signals  $x' \in \mathbb{R}^{H \times W \times C \times S}$ . The decoder  $f_{\text{dec}}(\cdot)$  is a function that maps sequential synaptic current signals  $x' \in \mathbb{R}^{H \times W \times C \times S}$  to an image  $x \in \mathbb{R}^{H \times W \times C}$ . Here, we refer to the original data space  $\mathbb{R}^{H \times W \times C}$  as the image space and the synaptic current signal space  $\mathbb{R}^{H \times W \times C \times S}$  as the signal space. The input of the SNN  $f_{\text{SNN}}$  is the synaptic current signals  $x'_t \in \mathbb{R}^{H \times W \times C \times S}$  and the step  $t \in \{1, \dots, T\}$ . The output is the synaptic current signals  $\hat{z}' \in \mathbb{R}^{H \times W \times C \times S}$ .

Using SNN  $f_{\text{SNN}}$ , encoder  $f_{\text{enc}}$  and decoder  $f_{\text{dec}}$ , the denoising step becomes

$$x_{t-1} = a_t x_t + b_t f_{\text{dec}}(f_{\text{SNN}}(f_{\text{enc}}(x_t), t)) \quad (13)$$

(Fig. 1b). The loss was calculated in the image space using Eq. (8).

$$L_{\text{ddpm}} = \sum_{t=1}^T \gamma_t \mathbb{E} \left[ \left\| z - f_{\text{dec}}(f_{\text{SNN}}(f_{\text{enc}}(x_t), t)) \right\|^2 \right] \quad (14)$$

$z$  is the target such as the noise  $\epsilon$ , original image  $x_0$ , or velocity  $v_t$ , which the SNN tries to estimate. Subsequently, we obtained a generative process using an SNN. However, it still requires encoding and decoding at each step of the generative process and cannot be completed by only SNNs. To solve this problem, we aim to calculate the generative process of DDIM in the signal space (Fig. 1d).

$$x'_{t-1} = a_t x'_t + b_t f_{\text{SNN}}(x'_t, t) \quad (15)$$

where  $x'_t$  and  $x'_{t-1}$  are corresponding signals to  $x_t$  and  $x_{t-1}$  in the signal space.

First, we propose the use of a linear encoder and decoder for  $f_{\text{enc}}$  and  $f_{\text{dec}}$  to compute the linear combination in the signal space (Fig. 1c). Because the encoder and decoder are linear maps, we can change the order of these operations and the linear combination. Therefore, we can rewrite Eq. (13) as follows:

$$x'_{t-1} = a_t x'_t + b_t f_{\text{enc}}(f_{\text{dec}}(f_{\text{SNN}}(x'_t, t))) \quad (16)$$

where  $x'_T = f_{\text{enc}}(x_T)$ .

Then, we can remove the decoding and encoding processes in Eq. (16) by approximating  $f_{\text{enc}}(f_{\text{dec}}(f_{\text{SNN}}(x'_t, t)))$  with  $f_{\text{SNN}}(x'_t, t)$  by minimizing the squared error  $L_{\text{scl}}$  between them at every step.

$$L_{\text{scl}} = \sum_{t=1}^T \lambda_t \mathbb{E} \left[ \left\| f_{\text{SNN}}(x'_t, t) - f_{\text{enc}}(f_{\text{dec}}(f_{\text{SNN}}(x'_t, t))) \right\|^2 \right] \quad (17)$$

$\lambda_t$  is a hyper-parameter. Consequently, we obtain Eq. (15).

We call the loss function  $L_{\text{scl}}$  the SCL loss and simultaneously minimize the SCL and diffusion losses Eq. (14). The total loss function  $L$  becomes:

$$L = L_{\text{ddpm}} + L_{\text{scl}} \quad (18)$$

### 3.3. Equivalence between synaptic currents and spike trains

Our denoising step involves the linear combination and subsequent convolution of real-valued synaptic currents. While recent works for SNNs accept non-binary multiply-add operations [17, 23, 34, 61], our model can be further equivalently regarded as processing only spike trains, as illustrated

in Fig. 3. The linear combination, as well as the first and last convolutions in the SNN, constitute affine maps and thus can be consolidated into a single convolutional layer.

### 3.4. Network architecture

We designed our SNN architecture based on the UNet used in DDPM [22] without self-attention. Instead of group normalization [54], we use tdbn [60]. We also added the time embeddings for step  $t$  to each ResNet block in our Spiking UNet following DDPM. We used direct input encoding [45] for time embeddings.

In the following section, we use direct input encoding [45] calculated independently of each pixel for encoder  $f_{\text{enc}}$ , which is defined as

$$f_{\text{enc}}(x_{ijk}) = (x_{ijk}, x_{ijk}, \dots, x_{ijk}) \quad (19)$$

where  $x_{ijk}$  denotes the pixel value of the input image at position  $(i, j)$  and channel  $k$ . The decoder  $f_{\text{dec}}$  is defined similarly to [60] as

$$f_{\text{dec}}(x_{ijk}^{(1:S)}) = \frac{1}{S} \sum_{s=1}^S x_{ijk}^{(s)} \quad (20)$$

where  $x_{ijk}^{(s)}$  is the output synaptic current of the index  $(i, j, k)$  at the time step  $s$ .

## 4. Experiment

We implemented our model using PyTorch [40] and trained it using MNIST [30], Fashion MNIST [57], CIFAR10 [29] and CelebA [36]. Because there are no other fully spiking diffusion models, we compared the evaluation metrics to FSVAE [25], the state-of-the-art VAE-based fully spiking generative model for SNNs.

### 4.1. Experimental settings

The thresholds  $V_{th}$  and  $\tau_{decay}$  were set to 1.0 and 0.8 respectively. During backpropagation, we use a detaching reset [58]. We used 4 or 8 as the number of time steps  $S$ . Generally, higher time steps have more expressive power; however, they also increase the computational cost and latency.

The diffusion model uses a cosine schedule [39, 47] with the number of steps  $T = 1000$ , and our Spiking UNet is trained to predict the velocity  $v_t$  following [47].

We used the Adam optimizer [28] with  $\beta_1 = 0.9$ ,  $\beta_2 = 0.999$  and  $\epsilon = 10^{-8}$  with a learning rate of 0.001 for MNIST and Fashion MNIST, and 0.0005 for CIFAR10 and CelebA. The batch size is 256.

For evaluation metrics of the quality of generated images, we used the same metrics as FSVAE [25], Fréchet inception distance (FID) [21] and Fréchet autoencoder distance (FAD). FAD is a metric used in FSVAE and is calculated by the Fréchet distance of a trained autoencoder’s

latent variables between samples and real images. They suggested the use of FAD because FID uses the output of Inception-v3 [52] trained on ImageNet [12] and it may not work in a different domain such as MNIST. We used the same autoencoder architecture as FSVAE for FAD. Following FSVAE, we used the test data of each dataset for evaluation: 10,000 images from MNIST, Fashion MNIST and CIFAR10, and 19,962 images from CelebA. We then generate 10,000 images for each dataset and the metrics were calculated.

### 4.2. Results

The evaluation results are presented in Tab. 1. We can see that FSDDIM outperforms FSVAE [25] in terms of FID and FAD for all datasets. Moreover, FSDDIM achieved much higher results with fewer time steps than FSVAE, which reduced the computational cost and latency. We successfully trained the model with 55.3M parameters, whereas Kamata *et al.* investigated relatively small models with a number of parameters up to 6.7M for FSVAE [25]. These results suggest that the superiority of diffusion models over VAEs is also valid in the case of SNNs.

In addition, we compared the FID with the existing SD-DPM [4] and Spiking-Diffusion [35] which are not fully spiking but diffusion models using SNNs. As a result, FSDDIM achieved better FID than that of both models on MNIST and Fashion MNIST, and than that of Spiking-Diffusion on CIFAR10. Therefore, FSDDIM is superior to these existing works not only in terms of the potential of the model to be seamlessly implemented on neuromorphic devices in the future, but also in terms of the quality of the generated images.

The images generated by FSVAE are shown in Fig. 4.

### 4.3. Ablation study

An ablation study is conducted to investigate the effects of the proposed SCL loss method. We trained our model with and without SCL loss on CIFAR10 and calculated FID with generated 5,000 images. We used time steps  $S = 8$ . In addition, we trained our model with another loss function  $L_{\text{signal}}$  instead of the SCL loss, which computes squared error of encoded target  $f_{\text{enc}}(z)$  and output of the SNN:

$$L_{\text{signal}} = \sum_{t=1}^T \lambda_t \|f_{\text{enc}}(z) - f_{\text{SNN}}(x'_t, t)\|^2 \quad (21)$$

If the DDPM loss  $L_{\text{ddpm}}$  in Eq. (14) is 0, then  $L_{\text{signal}}$  is equivalent to the SCL loss. Therefore, we compared the results of the model trained with  $L_{\text{signal}}$  or the SCL loss to investigate the effects of the SCL loss.

The results are presented in Tab. 2. We can see that the model trained with SCL loss achieved the highest performance; 48.75. The model trained without SCL loss

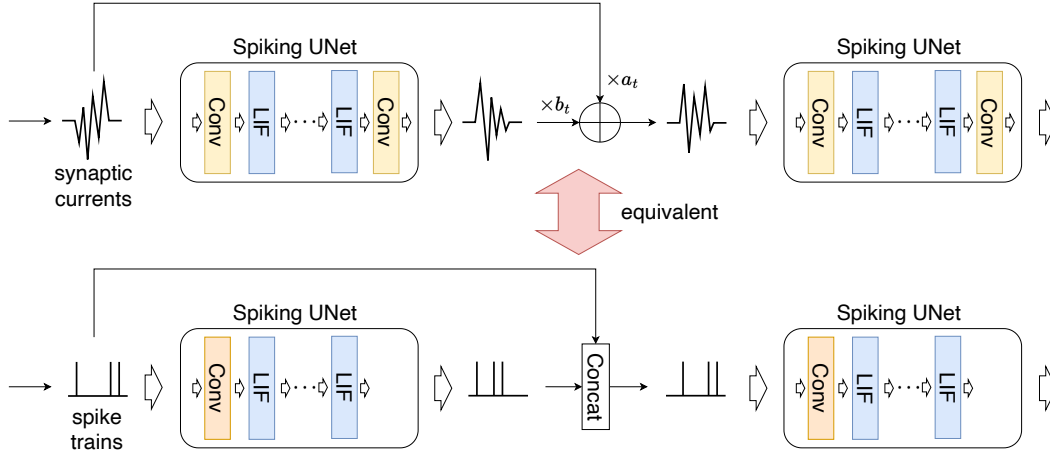


Figure 3. The conversion from the linear combination of synaptic currents to the channel-wise concatenation of spike trains. We can regard our model which outputs synaptic currents as a model which outputs spike trains by fusing the linear combination weights and the first and last convolutional layer into a single convolutional layer.

Dataset	Model	Time steps	FID ↓	FAD ↓
MNIST	SDDPM [4]	4	(29.48)	—
	Spiking-Diffusion [35]	16	(37.50)	—
	FSVAE [25]	16	57.77	36.52
	<b>FSDDIM (ours)</b>	8	<b>3.99</b>	5.71
	<b>FSDDIM (ours)</b>	4	7.48	<b>3.62</b>
Fashion MNIST	SDDPM [4]	4	(21.38)	—
	Spiking-Diffusion [35]	16	(91.98)	—
	FSVAE [25]	16	58.45	16.45
	<b>FSDDIM (ours)</b>	8	11.78	<b>4.91</b>
	<b>FSDDIM (ours)</b>	4	<b>9.17</b>	9.25
CIFAR10	SDDPM [4]	8	(16.89)	—
	SDDPM [4]	4	(19.20)	—
	Spiking-Diffusion [35]	16	(120.5)	—
	FSVAE [25]	16	175.7	139.97
	<b>FSDDIM (ours)</b>	8	<b>46.14</b>	12.61
<b>FSDDIM (ours)</b>	4	51.46	<b>8.63</b>	
CelebA	SDDPM [4]	4	(25.09)	—
	FSVAE [25]	16	101.5	113.15
	<b>FSDDIM (ours)</b>	4	<b>36.08</b>	<b>66.52</b>

Table 1. Comparison of FID and FAD on MNIST, Fashion MNIST, CIFAR10 and CelebA. Since SDDPM [4] and Spiking-Diffusion [35] are not fully spiking models, we show their results for only reference purpose, and we put the results in parentheses. Their results are taken from [4] and [35] respectively. The best results among fully spiking models are highlighted in bold.

achieved the worst performance; FID was 80.03.  $L_{\text{signal}}$  also improved the performance but the SCL loss was more effective than  $L_{\text{signal}}$ . Consequently, we can conclude that the SCL loss is effective for training our model.

#### 4.4. Computational cost

We implemented an ANN model with the same architecture as our Spiking UNet and calculated the number of additions and multiplications during the generation of an image to demonstrate the computational effectiveness of FSDDIM. The results are shown in Tab. 3. We can see that

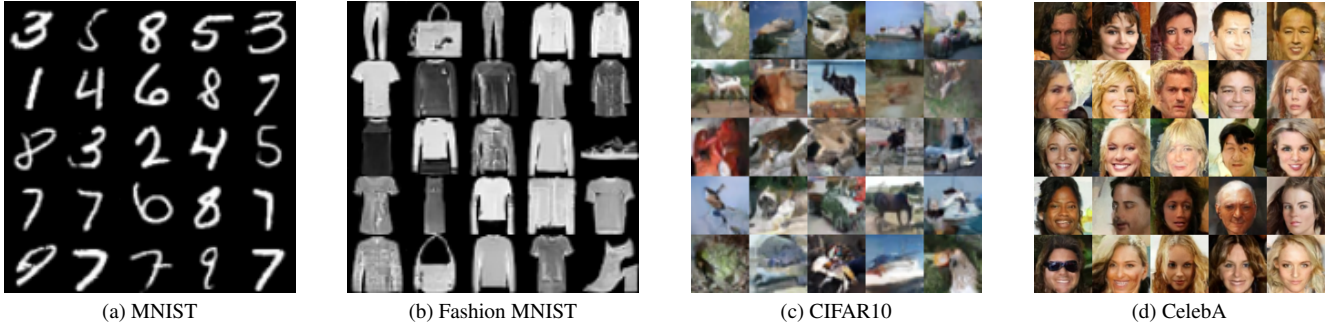


Figure 4. Generated images of MNIST, Fashion MNIST, CIFAR10 and CelebA. For CelebA, relatively good results are selected. The results on the other datasets are randomly sampled. The results of Fashion MNIST and CelebA are generated with 4 time steps. The results of MNIST and CIFAR10 are generated with 8 time steps.

Model	FID ↓
FSDDIM w/o $L_{scl}$	80.03
FSDDIM w/ $L_{scl}$	<b>48.75</b>
FSDDIM w/o $L_{scl}$ , w/ $L_{signal}$	50.33
FSDDIM w/ $L_{scl}$ , w/ $L_{signal}$	52.77

Table 2. Ablation study of the SCL loss on CIFAR10.

our model with 4 time steps reduces the number of multiplications by 74.1% and the number of additions by 14.9% compared with the ANN model. Our model with 8 time steps increased the number of additions, but still reduced the number of multiplications, which is generally more computationally expensive, by 48.1% compared with the ANN model. Therefore, our model exhibits computational efficiency compared with the ANN model, with the prospect of significant speedup and energy efficiency on neuromorphic devices. We leave the implementation on neuromorphic devices as future work.

Model	Time steps	#Addition	#Multiplication
ANN	—	$4.98 \times 10^{12}$	$4.97 \times 10^{12}$
<b>ours</b>	8	$7.14 \times 10^{12}$	$2.58 \times 10^{12}$
<b>ours</b>	4	<b><math>4.24 \times 10^{12}</math></b>	<b><math>1.29 \times 10^{12}</math></b>

Table 3. Computational cost of a single step of generative process on Fashion MNIST. The results are averaged over 100 images.

## 5. Conclusion

In this work, we proposed the FSDDIM which is a fully spiking diffusion model. This model was implemented via SCL, which uses synaptic currents instead of spike trains as model outputs. We introduced SCL loss by adopting a linear encoding and decoding scheme and showed that this SCL loss aids in completing the entire generative process of our

diffusion model exclusively using SNNs. The experimental results showed that our model outperformed the state-of-the-art fully spiking image generation model in terms of quality of the generated images and number of time steps. To the best of our knowledge, our proposed FSDDIM is the first ever reported fully spiking diffusion model.

## 6. Acknowledgement

This work was partially supported by JST Moonshot R&D Grant Number JPMJPS2011, CREST Grant Number JPMJCR2015 and Basic Research Grant (Super AI) of Institute for AI and Beyond of the University of Tokyo.

We would like to thank Yusuke Mori and Atsuhiro Noguchi for helpful discussions. We would also like to thank Lin Gu and Akio Hayakawa for their helpful comments on the manuscript.

## References

- [1] Jacob Austin, Daniel D Johnson, Jonathan Ho, Daniel Tarlow, and Rianne Van Den Berg. Structured denoising diffusion models in discrete state-spaces. *Advances in Neural Information Processing Systems*, 34:17981–17993, 2021. [1](#), [4](#)
- [2] Guillaume Bellec, Darjan Salaj, Anand Subramoney, Robert Legenstein, and Wolfgang Maass. Long short-term memory and learning-to-learn in networks of spiking neurons. *Advances in neural information processing systems*, 31, 2018. [3](#)
- [3] Andrew Brock, Jeff Donahue, and Karen Simonyan. Large scale GAN training for high fidelity natural image synthesis. In *7th International Conference on Learning Representations, ICLR 2019, New Orleans, LA, USA, May 6-9, 2019*. OpenReview.net, 2019. [1](#)
- [4] Jiahang Cao, Ziqing Wang, Hanzhong Guo, Hao Cheng, Qiang Zhang, and Renjing Xu. Spiking denoising diffusion probabilistic models. *arXiv preprint arXiv:2306.17046*, 2023. [1](#), [2](#), [4](#), [6](#), [7](#)
- [5] Natalia Caporale and Yang Dan. Spike timing-dependent



- plasticity: a hebbian learning rule. *Annu. Rev. Neurosci.*, 31: 25–46, 2008. 3
- [6] Andrew S Cassidy, Rodrigo Alvarez-Icaza, Filipp Akopyan, Jun Sawada, John V Arthur, Paul A Merolla, Pallab Datta, Marc Gonzalez Tallada, Brian Taba, Alexander Andreopoulos, et al. Real-time scalable cortical computing at 46 gigasynaptic ops/watt with  $\sim 100\times$  speedup in time-to-solution and  $\sim 100,000\times$  reduction in energy-to-solution. In *SC'14: Proceedings of the International Conference for High Performance Computing, Networking, Storage and Analysis*, pages 27–38. IEEE, 2014. 1
- [7] Ting Chen. On the importance of noise scheduling for diffusion models. *arXiv preprint arXiv:2301.10972*, 2023. 4
- [8] Yann Chérdo, Benoît Miramond, and Alain Pegatoquet. Time series prediction and anomaly detection with recurrent spiking neural networks. In *2023 International Joint Conference on Neural Networks (IJCNN)*, pages 1–10. IEEE, 2023. 2, 4
- [9] Jooyoung Choi, Jungbeom Lee, Chaehun Shin, Sungwon Kim, Hyunwoo Kim, and Sungroh Yoon. Perception prioritized training of diffusion models. In *Proceedings of the IEEE/CVF Conference on Computer Vision and Pattern Recognition*, pages 11472–11481, 2022. 1, 3, 4
- [10] Benjamin Cramer, Yannik Stradmann, Johannes Schemmel, and Friedemann Zenke. The heidelberg spiking data sets for the systematic evaluation of spiking neural networks. *IEEE Transactions on Neural Networks and Learning Systems*, 33(7):2744–2757, 2020. 3
- [11] Mike Davies, Narayan Srinivasa, Tsung-Han Lin, Gautham Chinya, Yongqiang Cao, Sri Harsha Choday, Georgios Dimou, Prasad Joshi, Nabil Imam, Shweta Jain, et al. Loihi: A neuromorphic manycore processor with on-chip learning. *Ieee Micro*, 38(1):82–99, 2018. 1
- [12] Jia Deng, Wei Dong, Richard Socher, Li-Jia Li, Kai Li, and Li Fei-Fei. Imagenet: A large-scale hierarchical image database. In *2009 IEEE conference on computer vision and pattern recognition*, pages 248–255. Ieee, 2009. 6
- [13] Prafulla Dhariwal and Alexander Nichol. Diffusion models beat gans on image synthesis. *Advances in neural information processing systems*, 34:8780–8794, 2021. 1, 3, 4
- [14] Peter U Diehl and Matthew Cook. Unsupervised learning of digit recognition using spike-timing-dependent plasticity. *Frontiers in computational neuroscience*, 9:99, 2015. 3
- [15] Patrick Esser, Robin Rombach, and Bjorn Ommer. Taming transformers for high-resolution image synthesis. In *Proceedings of the IEEE/CVF conference on computer vision and pattern recognition*, pages 12873–12883, 2021. 1
- [16] Steve K Esser, Rathinakumar Appuswamy, Paul Merolla, John V Arthur, and Dharmendra S Modha. Backpropagation for energy-efficient neuromorphic computing. *Advances in neural information processing systems*, 28, 2015. 3
- [17] Wei Fang, Zhaofei Yu, Yanqi Chen, Tiejun Huang, Timothée Masquelier, and Yonghong Tian. Deep residual learning in spiking neural networks. In *Advances in Neural Information Processing Systems 34: Annual Conference on Neural Information Processing Systems 2021, NeurIPS 2021, December 6-14, 2021, virtual*, pages 21056–21069, 2021. 4, 5
- [18] Wei Fang, Zhaofei Yu, Yanqi Chen, Timothée Masquelier, Tiejun Huang, and Yonghong Tian. Incorporating learnable membrane time constant to enhance learning of spiking neural networks. In *Proceedings of the IEEE/CVF international conference on computer vision*, pages 2661–2671, 2021. 3
- [19] Shuyang Gu, Dong Chen, Jianmin Bao, Fang Wen, Bo Zhang, Dongdong Chen, Lu Yuan, and Baining Guo. Vector quantized diffusion model for text-to-image synthesis. In *Proceedings of the IEEE/CVF Conference on Computer Vision and Pattern Recognition*, pages 10696–10706, 2022. 1, 3
- [20] Tiankai Hang, Shuyang Gu, Chen Li, Jianmin Bao, Dong Chen, Han Hu, Xin Geng, and Baining Guo. Efficient diffusion training via min-snr weighting strategy. *arXiv preprint arXiv:2303.09556*, 2023. 3, 4
- [21] Martin Heusel, Hubert Ramsauer, Thomas Unterthiner, Bernhard Nessler, and Sepp Hochreiter. Gans trained by a two time-scale update rule converge to a local nash equilibrium. *Advances in neural information processing systems*, 30, 2017. 6
- [22] Jonathan Ho, Ajay Jain, and Pieter Abbeel. Denoising diffusion probabilistic models. *Advances in neural information processing systems*, 33:6840–6851, 2020. 1, 3, 4, 6, 11, 12
- [23] Yifan Hu, Lei Deng, Yujie Wu, Man Yao, and Guoqi Li. Advancing spiking neural networks towards deep residual learning. *arXiv preprint arXiv:2112.08954*, 2021. 4, 5
- [24] Allan Jabri, David J. Fleet, and Ting Chen. Scalable adaptive computation for iterative generation. In *International Conference on Machine Learning, ICML 2023, 23-29 July 2023, Honolulu, Hawaii, USA*, pages 14569–14589. PMLR, 2023. 4
- [25] Hiromichi Kamata, Yusuke Mukuta, and Tatsuya Harada. Fully spiking variational autoencoder. In *Proceedings of the AAAI Conference on Artificial Intelligence*, pages 7059–7067, 2022. 1, 4, 6, 7
- [26] Tero Karras, Samuli Laine, Miika Aittala, Janne Hellsten, Jaakko Lehtinen, and Timo Aila. Analyzing and improving the image quality of stylegan. In *Proceedings of the IEEE/CVF conference on computer vision and pattern recognition*, pages 8110–8119, 2020. 1
- [27] Jaehyun Kim, Heesu Kim, Subin Huh, Jinho Lee, and Kiyoung Choi. Deep neural networks with weighted spikes. *Neurocomputing*, 311:373–386, 2018. 2, 4
- [28] Diederik P. Kingma and Jimmy Ba. Adam: A method for stochastic optimization. In *3rd International Conference on Learning Representations, ICLR 2015, San Diego, CA, USA, May 7-9, 2015, Conference Track Proceedings*, 2015. 6
- [29] Alex Krizhevsky, Geoffrey Hinton, et al. Learning multiple layers of features from tiny images. 2009. 6
- [30] Yann LeCun, Léon Bottou, Yoshua Bengio, and Patrick Haffner. Gradient-based learning applied to document recognition. *Proceedings of the IEEE*, 86(11):2278–2324, 1998. 3, 6
- [31] Chankyu Lee, Syed Shakib Sarwar, Priyadarshini Panda, Gopalakrishnan Srinivasan, and Kaushik Roy. Enabling spike-based backpropagation for training deep neural network architectures. *Frontiers in neuroscience*, page 119, 2020. 2, 4

- [32] Jun Haeng Lee, Tobi Delbruck, and Michael Pfeiffer. Training deep spiking neural networks using backpropagation. *Frontiers in neuroscience*, 10:508, 2016. **3**
- [33] Robert Legenstein, Christian Naeger, and Wolfgang Maass. What can a neuron learn with spike-timing-dependent plasticity? *Neural computation*, 17(11):2337–2382, 2005. **3**
- [34] Lin Li and Yang Liu. Multi-dimensional attention spiking transformer for event-based image classification. In *2023 5th International Conference on Communications, Information System and Computer Engineering (CISCE)*, pages 359–362. IEEE, 2023. **5**
- [35] Mingxuan Liu, Rui Wen, and Hong Chen. Spiking-diffusion: Vector quantized discrete diffusion model with spiking neural networks. *arXiv preprint arXiv:2308.10187*, 2023. **1, 2, 4, 6, 7**
- [36] Ziwei Liu, Ping Luo, Xiaogang Wang, and Xiaoou Tang. Deep learning face attributes in the wild. In *Proceedings of International Conference on Computer Vision (ICCV)*, 2015. **6**
- [37] Chenlin Meng, Robin Rombach, Ruiqi Gao, Diederik Kingma, Stefano Ermon, Jonathan Ho, and Tim Salimans. On distillation of guided diffusion models. In *Proceedings of the IEEE/CVF Conference on Computer Vision and Pattern Recognition*, pages 14297–14306, 2023. **4**
- [38] Eliya Nachmani, Robin San Roman, and Lior Wolf. Non gaussian denoising diffusion models. *arXiv preprint arXiv:2106.07582*, 2021. **1**
- [39] Alexander Quinn Nichol and Prafulla Dhariwal. Improved denoising diffusion probabilistic models. In *International Conference on Machine Learning*, pages 8162–8171. PMLR, 2021. **1, 3, 4, 6**
- [40] Adam Paszke, Sam Gross, Francisco Massa, Adam Lerer, James Bradbury, Gregory Chanan, Trevor Killeen, Zeming Lin, Natalia Gimelshein, Luca Antiga, et al. Pytorch: An imperative style, high-performance deep learning library. *Advances in neural information processing systems*, 32, 2019. **6**
- [41] Junran Pu, Wang Ling Goh, Vishnu P Nambiar, Ming Ming Wong, and Anh Tuan Do. A 5.28-mm<sup>2</sup> 4.5-pj/sop energy-efficient spiking neural network hardware with reconfigurable high processing speed neuron core and congestion-aware router. *IEEE Transactions on Circuits and Systems I: Regular Papers*, 68(12):5081–5094, 2021. **1**
- [42] Robin Rombach, Andreas Blattmann, Dominik Lorenz, Patrick Esser, and Björn Ommer. High-resolution image synthesis with latent diffusion models. In *Proceedings of the IEEE/CVF conference on computer vision and pattern recognition*, pages 10684–10695, 2022. **1, 3, 4**
- [43] Olaf Ronneberger, Philipp Fischer, and Thomas Brox. U-net: Convolutional networks for biomedical image segmentation. In *Medical Image Computing and Computer-Assisted Intervention—MICCAI 2015: 18th International Conference, Munich, Germany, October 5–9, 2015, Proceedings, Part III 18*, pages 234–241. Springer, 2015. **4, 11**
- [44] Kaushik Roy, Akhilesh Jaiswal, and Priyadarshini Panda. Towards spike-based machine intelligence with neuromorphic computing. *Nature*, 575(7784):607–617, 2019. **1**
- [45] Bodo Rueckauer, Iulia-Alexandra Lungu, Yuhuang Hu, Michael Pfeiffer, and Shih-Chii Liu. Conversion of continuous-valued deep networks to efficient event-driven networks for image classification. *Frontiers in neuroscience*, 11:682, 2017. **6, 11**
- [46] Chitwan Saharia, William Chan, Saurabh Saxena, Lala Li, Jay Whang, Emily L Denton, Kamyar Ghasemipour, Raphael Gontijo Lopes, Burcu Karagol Ayan, Tim Salimans, et al. Photorealistic text-to-image diffusion models with deep language understanding. *Advances in Neural Information Processing Systems*, 35:36479–36494, 2022. **1, 3, 4**
- [47] Tim Salimans and Jonathan Ho. Progressive distillation for fast sampling of diffusion models. In *The Tenth International Conference on Learning Representations, ICLR 2022, Virtual Event, April 25–29, 2022*. OpenReview.net, 2022. **3, 4, 6**
- [48] Tim Salimans, Andrej Karpathy, Xi Chen, and Diederik P Kingma. Pixelcnn++: Improving the pixelcnn with discretized logistic mixture likelihood and other modifications. *arXiv preprint arXiv:1701.05517*, 2017. **4, 11**
- [49] Jiaming Song, Chenlin Meng, and Stefano Ermon. Denoising diffusion implicit models. *arXiv preprint arXiv:2010.02502*, 2020. **1, 2, 3, 4**
- [50] RB Stein and Alan Lloyd Hodgkin. The frequency of nerve action potentials generated by applied currents. *Proceedings of the Royal Society of London. Series B. Biological Sciences*, 167(1006):64–86, 1967. **3**
- [51] Qiaoyi Su, Yuhong Chou, Yifan Hu, Jianing Li, Shijie Mei, Ziyang Zhang, and Guoqi Li. Deep directly-trained spiking neural networks for object detection. In *Proceedings of the IEEE/CVF International Conference on Computer Vision*, pages 6555–6565, 2023. **4**
- [52] Christian Szegedy, Vincent Vanhoucke, Sergey Ioffe, Jon Shlens, and Zbigniew Wojna. Rethinking the inception architecture for computer vision. In *Proceedings of the IEEE conference on computer vision and pattern recognition*, pages 2818–2826, 2016. **6**
- [53] Xiangwen Wang, Xianghong Lin, and Xiaochao Dang. Supervised learning in spiking neural networks: A review of algorithms and evaluations. *Neural Networks*, 125:258–280, 2020. **1**
- [54] Yuxin Wu and Kaiming He. Group normalization. In *Proceedings of the European conference on computer vision (ECCV)*, pages 3–19, 2018. **6**
- [55] Yujie Wu, Lei Deng, Guoqi Li, Jun Zhu, and Luping Shi. Spatio-temporal backpropagation for training high-performance spiking neural networks. *Frontiers in neuroscience*, 12:331, 2018. **3**
- [56] Yujie Wu, Lei Deng, Guoqi Li, Jun Zhu, Yuan Xie, and Luping Shi. Direct training for spiking neural networks: Faster, larger, better. In *Proceedings of the AAAI conference on artificial intelligence*, pages 1311–1318, 2019. **3**
- [57] Han Xiao, Kashif Rasul, and Roland Vollgraf. Fashion-mnist: a novel image dataset for benchmarking machine learning algorithms, 2017. **6**
- [58] Friedemann Zenke and Tim P Vogels. The remarkable robustness of surrogate gradient learning for instilling complex

function in spiking neural networks. *Neural computation*, 33 (4):899–925, 2021. 3, 6

- [59] Wenrui Zhang and Peng Li. Spike-train level backpropagation for training deep recurrent spiking neural networks. *Advances in neural information processing systems*, 32, 2019. 3
- [60] Hanle Zheng, Yujie Wu, Lei Deng, Yifan Hu, and Guoqi Li. Going deeper with directly-trained larger spiking neural networks. In *Thirty-Fifth AAAI Conference on Artificial Intelligence, AAAI 2021, Thirty-Third Conference on Innovative Applications of Artificial Intelligence, IAAI 2021, The Eleventh Symposium on Educational Advances in Artificial Intelligence, EAAI 2021, Virtual Event, February 2-9, 2021*, pages 11062–11070. AAAI Press, 2021. 2, 4, 6, 11
- [61] Zhaokun Zhou, Yuesheng Zhu, Chao He, Yaowei Wang, Shuicheng Yan, Yonghong Tian, and Li Yuan. Spikformer: When spiking neural network meets transformer. In *The Eleventh International Conference on Learning Representations, ICLR 2023, Kigali, Rwanda, May 1-5, 2023*. OpenReview.net, 2023. 5

## Supplementary Material

### A. Implementation details

#### A.1. Model architecture

Following DDPM [22], we employ a UNet [43, 48] as the neural network to estimate the target in each denoising step. The architecture of our Spiking UNet is illustrated in Fig. 5. The Spiking UNet comprises four downsampling blocks and four upsampling blocks. Each block consists of two ResBlocks and a downsampling or upsampling layer, except for the last downsampling and upsampling blocks, which contain two ResBlocks and a convolutional layer with tdBN [60] and LIF layers. We incorporate time embeddings into the ResBlocks, similar to DDPM. Using sinusoidal time embeddings with 512 dimensions, these embeddings are introduced via direct input encoding [45] into two linear layers with tdBN and LIF layers. The embeddings are then projected and added in each ResBlock. The number of channels in each downsampling block is 128, 256, 384, and 512, respectively. Conversely, the number of channels in each upsampling block is 512, 384, 256, and 128. Before the initial downsampling block, a convolutional layer with a channel size of 128 is added. After the final upsampling block, a ResBlock with a channel size of 128 and a convolutional layer with a channel size of 1 or 3 (depending on the dataset) is added. The convolutional layer in each ResBlock has a kernel size of  $3 \times 3$ , a stride of  $1 \times 1$ , and a padding of  $1 \times 1$ . The downsampling layer consists of an average pooling layer with a kernel size of  $2 \times 2$  and a stride of  $2 \times 2$ , followed by a convolutional layer with a kernel size of  $1 \times 1$ . In the upsampling blocks, we utilize a nearest neighbor upsampling layer with a scale factor of  $2 \times 2$  and

a convolutional layer with a kernel size of  $3 \times 3$ . The input of each ResBlock is concatenated with the output of the corresponding downsampling block, following the DDPM approach. The input of the final convolutional layer is concatenated with the output of all ResBlocks with the same resolution. In the inference phase, the subsequent convolutional layers after downsampling and upsampling layers can be fused into a single convolutional layer.

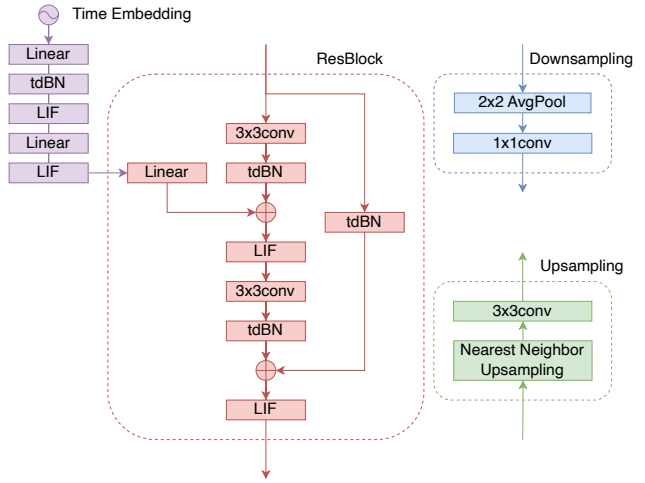
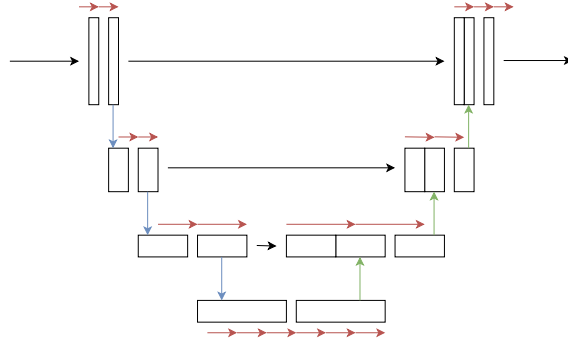


Figure 5. Model architecture.

#### A.2. Training details

The images from MNIST, Fashion MNIST, and CIFAR10 were resized to  $32 \times 32$ . CelebA images were cropped to  $148 \times 148$  and then resized to  $64 \times 64$ . We utilized 60,000 images for training from MNIST and Fashion MNIST, 50,000 images from CIFAR10, and 162,770 images from CelebA. For MNIST, Fashion MNIST, and CIFAR10, the entire training set was used per epoch. In the case of CelebA, 51,200 images were randomly selected from the training set for each epoch. The model was trained for 1,500 epochs, with FID calculated every 150 epochs using 1,000 generated images. The best model, determined by FID, was selected for the final evaluation. We set the hyper-



Figure 6. Generated images on MNIST.

parameters  $\gamma_t$  in Eq. (14) to  $\gamma_t = \bar{\alpha}_t$  for all  $t$ , following the same weighting as DDPM [22] when the target  $z$  is the velocity  $v_t$ . The hyper-parameters  $\lambda_t$  in Eq. (14) were set to  $\lambda_t = b_t/S$  for all  $t$ . We employed Monte Carlo method to minimize the loss in both Eq. (14) and Eq. (17), following the approach of DDPM. The training algorithm is presented in Algorithm 1.

---

**Algorithm 1: Training Algorithm**

---

```

1 repeat
2    $x_0 \sim q(x_0)$ 
3    $t \sim \text{Uniform}(\{1, \dots, T\})$ 
4    $\epsilon \sim \mathcal{N}(0, I)$ 
5    $x_t \leftarrow \sqrt{\bar{\alpha}_t}x_0 + \sqrt{1 - \bar{\alpha}_t}\epsilon$ 
6    $v_t \leftarrow \sqrt{\bar{\alpha}_t}\epsilon - \sqrt{1 - \bar{\alpha}_t}x_0$ 
7    $\hat{v} \leftarrow f_{\text{SNN}}(f_{\text{enc}}(x_t), t)$ 
8    $l_{\text{ddpm}} \leftarrow \|v_t - f_{\text{dec}}(\hat{v})\|^2$ 
9    $l_{\text{scl}} \leftarrow \|\hat{v} - f_{\text{enc}}(f_{\text{dec}}(\hat{v}))\|^2$ 
10  Take gradient descent step on
       $\nabla_{\theta}(\gamma_t l_{\text{ddpm}} + \lambda_t l_{\text{scl}})$ 
11 until converged;
```

---

## B. Generated images

We show additional generated images of our model in Fig. 6, Fig. 7, Fig. 8 and Fig. 9.



Figure 7. Generated images on Fashion MNIST.



Figure 8. Generated images on CIFAR10.

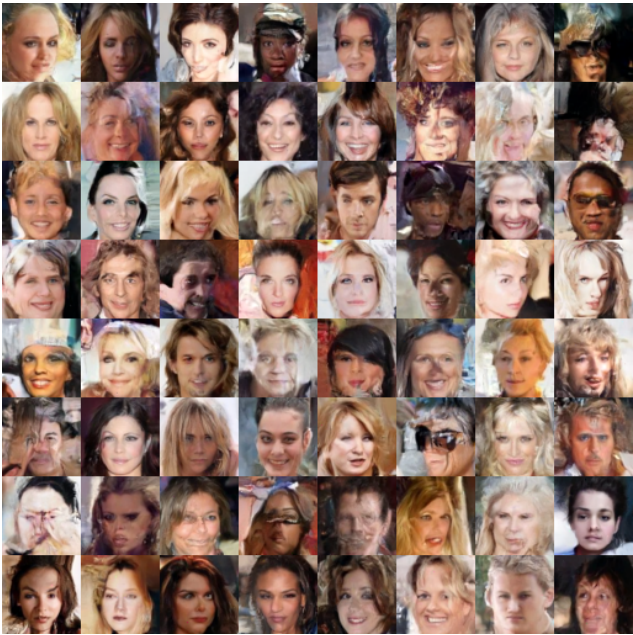


Figure 9. Generated images on CelebA.